Article

Not peer-reviewed version

Conventional Manufacturing by Pouring versus Additive Manufacturing Technology of β-Tricalcium Phosphate Bone Substitute Implants

Tanja Zöller , Hagen Schmal , Matthias Ahlhelm , Hermann O Mayr , Michael Seidenstuecker *

Posted Date: 9 May 2024

doi: 10.20944/preprints202405.0547.v1

Keywords: Sintering; β-TCP; additive manufacturing; Freeze Foam; hybrid bone; biocompatibility; bone replacement

Article

Conventional Manufacturing by Pouring Versus Additive Manufacturing Technology of β-tricalcium Phosphate Bone Substitute Implants

Tanja Zöller [1], Hagen Schmal [2], Matthias Ahlhelm [3], Hermann O. Mayr [2] and Michael Seidenstuecker [1,2,*]

[1] G.E.R.N. Tissue Replacement, Regeneration & Neogenesis, Department of Orthopedics and Trauma Surgery, Medical Center-Albert-Ludwigs-University of Freiburg, Faculty of Medicine, Albert-Ludwigs-University of Freiburg, Hugstetter Straße 55, 79106 Freiburg, Germany;
[2] Department of Orthopedics and Trauma Surgery, Medical Center-Albert-Ludwigs-University of Freiburg, Faculty of Medicine, Albert-Ludwigs-University of Freiburg, Hugstetter Straße 55, 79106 Freiburg, Germany
[3] Fraunhofer Institute for Ceramic Technologies and Systems, IKTS, Winterbergstraße 28, 01277 Dresden, Germany
* Correspondence: michael.seidenstuecker@uniklinik-freiburg.de

Abstract: The aim of the study was the comparison of conventional sintering versus additive manufacturing techniques for β-TCP bioceramics, focusing on mechanical properties and biocompatibility. A "critical" bone defect requires surgical intervention beyond simple stabilization. Autologous bone grafting is the gold standard treatment for such defects but it has its limitations. Alloplastic bone grafting using synthetic materials is becoming increasingly popular. The use of bone graft substitutes has increased significantly and current research was focused on optimizing these substitutes, whereas this study compares two existing manufacturing techniques and the thereby produced β-TCP implants. The 3D-printed β-TCP hybrid structure implant was fabricated using two components, a column structure and a freeze-foam, which were sintered together. The conventionally manufactured ceramics were made by pouring. Both scaffolds were characterized according to porosity, mechanical properties and biocompatibility. The hybrid structure had a total porosity of 74.4 ± 0.5%. Microporous β-TCP implants had a porosity of 43.5 ± 2.4%, while macroporous β-TCP implants had a porosity of 61.81%. Mechanical testing revealed that the hybrid structure had a compressive strength of 10.4 ± 6 MPa, significantly lower than the microporous β-TCP implant's with 32.9 ± 8.7 MPa. Biocompatibility evaluations showed a steady increase in cell proliferation over time for all β-TCP implants, with minimal cytotoxicity. This study provides valuable insight into the potential of additive manufacturing for β-TCP bioceramics in the treatment of bone defects.

Keywords: Sintering; β-TCP; additive manufacturing; Freeze Foam; hybrid bone; biocompatibility; bone replacement

1. Introduction

There is no consensus on the definition of a "critical" bone substance defect; in general, it is understood to be a bone substance defect of such an extent that it would not heal spontaneously and therefore requires surgical intervention that goes beyond stabilization of the bone by means of osteosynthesis, for example by means of autologous bone grafting [1]. The underlying causes of relevant bone substance defects are varied. In most cases, the defect occurs due to debridement after blunt force trauma, when non-vital bone fragments are being removed. Sharp force can also directly lead to bone substance loss [2]. The etiology of bone substance defects also includes the excision of bone tumors and debridement following bone infections. Although bone tumors themselves have their highest incidence in the 10-14 age group at 10.6% [3], bone is the third most common site for

 doi:10.20944/preprints202405.0547.v1

metastases of solid primary tumors, including bronchial, colorectal, prostate and breast cancers [4], which can cause pathological fractures, making bone defect treatment necessary [5]. The current gold standard in the treatment of bone substance defects is still autologous bone grafts [6]. This involves harvesting the patient's own bone from another site, often the iliac crest, and transplanting it to the defect site. In 2021, 43,118 bone grafts were harvested across Germany [7]. However, this treatment method causes a so-called donor site defect, which is associated with considerable postoperative morbidity and can cause chronic pain at the donor site [8,9]. The amount of autologous bone available for transplantation is very limited. The second surgical field is also associated with an increased risk of postoperative wound infection [9]. In addition, bone graft harvesting results in a longer operation time and thus an increase in the risks associated with general anesthesia for patients, primarily cardiovascular, respiratory and renal complications [10]. The costs of bone defect therapy also increase due to the prolonged duration of surgery; taking into account anesthesia, including medication and personnel as well as the surgical team and materials, the additional costs per operation amount to hundreds of euros [11]. These disadvantages can be avoided with alloplastic bone replacement; this involves the transplantation of synthetic foreign material. The relative use of bone graft substitutes in the treatment of bone substance defects increased significantly: from 11.8% in 2008 (10,163 cases in total) to 23.9% in 2018 (23,838 cases in total) [12]. Optimization of these bone substitutes is the subject of current research, including studies on the release of growth factors through the material [13–15] or the integration of stem cells into the material [13,15–17]. Bone graft substitutes are already being used in a variety of specialties, including orthopedics, dentistry, and oral and maxillofacial surgery. The use of metals to make plates, screws, and endoprostheses is common in orthopedics, with titanium being the most commonly used material, followed by magnesium and strontium [13]. In endodontics, bio-ceramics are used for various procedures such as root canal sealing [18]. In orthopedics, bioceramics are utilized to treat traumatic defects, such as fractures of the tibia, acetabulum, or distal radius [19–21], and to fill defects after resection of benign bone tumors [19,22,23]. These bioceramics are mostly based on calcium phosphates such as hydroxyapatite or beta-tricalcium phosphate (β-TCP). This paper will focus on the latter. Conventional sintering will be compared with current additive manufacturing techniques and the results will be evaluated in terms of mechanical strength and biocompatibility.

2. Materials and Methods

2.1. Materials

Pure ethanol was purchased from VWR International (VWR International GmbH, Darmstadt, Germany). Rat-tail collagen type I (dissolved in 0.02 N acetic acid, pH 3.3) was purchased from Corning (Corning, New York, NY, USA). Dulbecco's Modified Eagle medium nutrient mixture (DMEM/F12), penicillin/streptomycin, Dulbecco's phosphate-buffered saline (PBS), trypsin-EDTA 0.5% and trypan blue staining were purchased from Gibco (Grand Island, NE, USA). Ethidium D-III and calcein-AM were purchased as part of a live/dead cell staining II kit (PromoCell, Heidelberg, Germany). MG-63 (ATCC-CRL 1427) cells were purchased from ATCC. The cell proliferation reagent WST-I was purchased from Roche Diagnostics (Basel, Switzerland). LDH Assay (Cytotoxicity Detection Kit) was purchased by Sigma, now Merck (Darmstadt, Germany)

2.2. Manufacturing Processes Used

2.2.1. Manufacturing via Sintering of the β-TCP Ceramics Used

An established manufacturing method for β-TCP implants, which allows for their use as bone anchors in ACL reconstruction and as bone replacement [24,25] consists of the following steps. The industrially produced β-TCP was mixed with a porogen by pouring, then sintered, calcined and cleaned. The green body was prepared by mixing α-TCP and TCP (Merck AG, Zug, Switzerland) in a ratio of 4:1 and adding polyacrylic acid (Art. No. 81132, Fluka, Switzerland; MW = 5.1 kDa) as a porogen. It was then sintered at 1250°C for 4 hours at a heating and cooling rate of 1°C/min. Finally,

 doi:10.20944/preprints202405.0547.v1

the green body was calcined at a temperature of 900°C to remove any organic residues and cleaned with ethanol to remove combustion residues [26]. This manufacturing method was used in the industrial production of β-TCP implants in the above-mentioned procedure; accordingly, it is defined as a conventional manufacturing process in this paper [24]. Due to its use as a press-fit anchorage in the bone, this β-TCP implant is shaped like a cylinder with a diameter of 7 mm, a total length of 25 mm and a rounded end (cylindrical part with a length of 21.5 mm). According to the medical classification, it is a microporous β-TCP due to the average pore size of 5 µm, and therefore this implant will henceforth also be referred to as a microporous β-TCP implant.

2.2.2. Additive manufacturing of the β-TCP Ceramics Used

The 3D-printed β-TCP implant consists of two components that are joined together in the final manufacturing step and will therefore be referred to as a hybrid structure. Both components are made of hydroxyapatite calcined at 900°C for 2 hours. First, the column structure is fabricated using Ceramic Additive Manufacturing Vat Photopolymerization (VPP). The calcined hydroxyapatite is mixed with solvent, a mixture of synthetic resins and a photoinitiator. This suspension can now be solidified layer by layer using a UV laser, with a projection of the contours of the desired scaffold replacing a template [27]. The second component of the hybrid structure is a freeze foam. This is produced by foaming a suspension of the ceramic powder, water, a solvent, polyvinyl alcohol as a binder, and an additive for modified rheological properties and pH in a freeze dryer by lowering the ambient pressure and then freezing it. When the ambient pressure is further reduced, the frozen water sublimates and a solid ceramic foam is formed after subsequent heat treatment [27]. To implement the hybridization, the freeze-foam suspension was placed in cylindrical rubber molds, the columnar structure was inserted, and both were placed in the freeze dryer for the freeze-foaming process. Finally, the final hybrid structure was sintered in the same manner as the conventionally fabricated β-TCP implant. Sintering was performed at 1026.85°C (1300 K) for 1.5 hours after pre-sintering the columnar structure to compensate for its shrinkage during sintering. In this step, the initial hydroxyapatite is transformed into β-TCP. The structure and the two components of the hybrid structure are modeled on the architecture of human bone, which consists of solid cortical bone as the outer framework and the internal latticework of cancellous bone [27].

2.3. Characterization of the Resulting β-TCP Scaffolds

2.3.1. Characterization of Porosity

Micro-computed tomography: The acquisition of micro-computed tomography images of the microporous β-TCP implant and the macroporous, cylindrical β-TCP implant from curasan (curasan AG, Kleinostheim, Germany) of the 3D-printed β-TCP implant allows clear size characterization and mapping of the pore distribution. The "Foam Structure Analysis" software VGStudio Max v3.0 (Volume Graphics GmbH, Heidelberg) was used to precisely determine the porosity of the hybrid structure based on computed tomography images. The required computed tomography images were acquired with the CT-Compact (Procon X-ray GmbH, Sarstedt, Germany). Mercury porosimetry: Porosimetry, performed with the Pascal 140 and 440 mercury porosimeters (Porotec 140/440, POROTEC GmbH, Hofheim, Germany), allows the porosity of the microporous β-TCP implant to be precisely determined and the pore size to be measured. The measurements were performed as described elsewhere [28].

2.3.2. Mechanical Testing

The compression test was performed on a Zwick ZMART.PRO universal testing machine (ZwickRoell GmbH & Co. KG, Ulm, Germany) with a 20 kN load cell according to DIN 51104:2010-08. Data were collected using Zwick's testXpert II (version 3.7.1). The following parameters were used: Test speed 1 mm/min (position controlled), upper force limit of 8000 N and maximum deformation of 50%. Three specimens each were measured, with the macroporous cylindrical β-TCP implant from curasan (Cerasorb M, curasan AG, Kleinostheim) and the microporous β-TCP implant

 doi:10.20944/preprints202405.0547.v1

both tested with a height of 20 mm and cut to a height of 6 mm. The samples were cut to the appropriate height using an EXAKT diamond band saw (EXAKT Advanced Technologies GmbH, Norderstedt, Germany).

2.3.3. Degradation tests

Three samples each were stored in 5 ml Tris buffer with a pH value of 7.4 or additionally with a pH value of 5 for 60 days to simulate the effects of an inflammatory reaction in the body at 37°C in a Memmert drying oven (Memmert GmbH & Co. KG, Schwabach). The Tris buffer used was prepared according to the standard DIN EN ISO 10993-14 by dissolving 26.5 g of Tris in 1 liter of double-distilled water, adjusting the pH to the desired values first with 10 mol/l HCl, then with 1 mol/l HCl and 1 mol/l NaOH, and then checking it with a WTW inoLab 7110 pH meter (Xylem Analytics Germany Sales GmbH & Co. KG, Weilheim)[28].

2.3.4. Biocompatibility

MG-63 cells (ATCC, CRL 1427) were used for all biocompatibility testing. All tests were performed with 50,000 cells/100 µL per scaffold. Per test, 10 identical scaffolds per geometry variation were used and all tests were repeated at least 3 times.

Live/Dead Assay

On each scaffold and on Thermanox coverslips as a control, 100 µL of medium was pipetted with 50,000 MG-63 cells/100 µL. The well plates were then incubated for 2 hours at 37°C and 5% CO2 saturation in an incubator. After two hours, 1 mL of the specific cell medium described above was added to each well before the well plates were incubated in the incubator for 3, 7, and 10 days. The staining solution was prepared by adding 2 mL DPBS (Art. No. 14190-094, Gibco, Grand Island, NE, USA) to a Falcon tube (Greiner Bio-One International GmbH, Kremsmünster, Austria) and 4 µL ethidium homodimer III (Eth D-III) solution (together with the calcein part of the Live/Dead Cell Staining Kit II (PromoCell, Heidelberg, Germany)) according to the manufacturer's protocol (PromoCell). After mixing the staining solution, 1 µL of calcein dye was added. All steps were performed in the dark to avoid photobleaching of the staining solution and samples. To eliminate serum esterase activity, the medium was removed from all samples at a given time point and the cells were washed. Staining was then performed according to a previously published protocol [27]. Evaluation was performed using an Olympus fluorescence microscope (BX51, Olympus, Osaka, Japan) at 5 different positions on the samples at 5x and 10x magnification.

Cell Proliferation (WST-I)

Cells were again seeded onto the scaffolds and, as a control, onto Thermanox coverslips in the same number and concentration as in the previous biocompatibility tests. After two hours of incubation in the incubator at 37°C and 5% CO2 saturation, the cells adhered to the scaffolds and Thermanox coverslips (as a control), allowing the appropriate medium (1 mL) to be added. Plates were then incubated in the incubator for 3, 7, and 10 days. For this purpose, all medium was aspirated, and all wells were washed three times with PBS. The scaffolds and Thermanox coverslips were then transferred to a new 24-well plate. In the old well plate, 300 µL of DMEM medium without phenol red (supplements: 1% FBS and 1% P/S) was added to each of the wells where the scaffolds and membranes were previously located. In the new well plate, 600 µL of the same medium was added to each of the wells containing the scaffolds and membranes. The blank contained only DMEM medium without phenol red (with the same additives) and was measured to account for background absorbance. Finally, 10% WST was added to all samples at each time point (3, 7, 10 d) and incubated for 2 hours. After 2 h, the absorbance was measured using a spectrometer at λ= 450 nm.

Cytotoxicity (LDH Assay)

LDH measurements were performed at 24, 48, and 72 h. In addition to the scaffolds, positive controls (Triton X, 100% toxicity) and negative controls (cells only, 0% toxicity) were used for measurements at different times. Both coated and uncoated scaffolds were used. Cells were seeded onto the scaffolds and membranes in 100 µL of their medium (MG-63: 50,000 cells/100 µL). These were then incubated for 2 hours in an incubator at 37 ◦C and 5% CO2 saturation. Subsequently, 1 mL

 doi:10.20944/preprints202405.0547.v1

of DMEM-F12 medium without phenol red was added to all wells with the addition of 1% P/S and 1% FBS. Since higher concentrations of FBS may induce background absorbance, only 1% FBS was used. In the positive controls (C+), an additional 1% Triton X-100 was added to kill 100% of the cells. After 24 h incubation in the incubator, 100 µL from each well were transferred to three new wells of a 96-well plate. Thus, 3 wells of 100 µL each were obtained from 1 well. To ensure that the "blank" had the same concentration of phenol red, 100 µL of DMEM-F12 medium containing phenol red was added to this well prior to transfer. To assess cytotoxicity, the Cytotoxicity Detection Kit solution was prepared. For this, 111.1 µL of catalyst solution was mixed with 5 mL of staining solution. Of this, 100 µL was pipetted into each well before the well plate was incubated in the dark for 30 minutes. At the end of the 30-minute period, the absorbance at 490 nm was measured using a spectrometer. The experiment was performed a total of 4 times.

2.4. Statistics

All values in this paper are expressed as mean ± standard deviation. Calculations were performed using Origin 2023 Professional SR1 (OriginLab, Northampton, MA, USA). The Shapiro-Wilcox test was used for determination of normal distribution, followed by ANOVA (Tukey test) for significance test ($p < 0.05$).

3. Results

The different scaffolds shown in the following Figure 1 (β-TCP RMS; β-TCP Curasan; hybrid structure) were used for all further investigations.

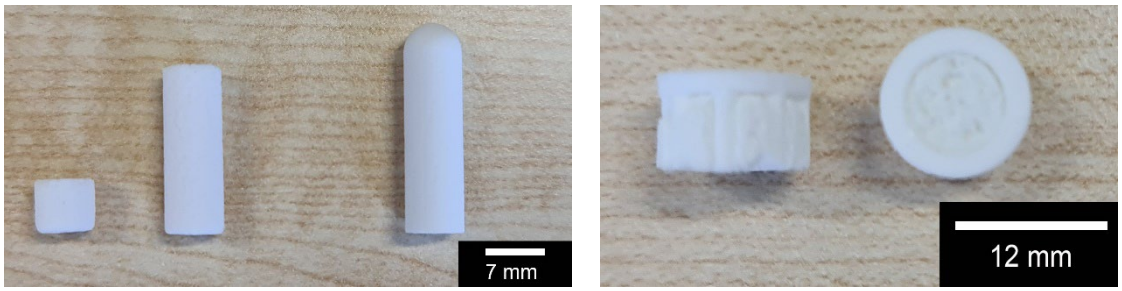

Figure 1. Overview of the scaffolds used: A: macroporous β-TCP from Curasan (6 and 20 mm length) left and center; microporous β-TCP from RMS; B: hybrid structure, side and top view.

3.1. Porosity

The total porosity of the hybrid structure, including the differential porosity of the column structure and the freeze foam, was 74.4 ± 0.5%. The microporous β-TCP implant showed a porosity of 43.5 ± 2.4% in mercury porosimetry, while that of the macroporous β-TCP implant was 61.81%. An average pore radius of 2.69 µm was determined for the microporous β-TCP implant, with a scatter range between 2 and 5 µm. The average pore radius of the macroporous β-TCP implant was 18.5 µm, with a range of 3 to 80 µm.

3.2. Mechanical Properties

When examining the compressive strength, there was a significant difference ($p<0.05$) between the hybrid structure with a compressive strength of 10.4 ± 6 MPa and the two microporous β-TCP implants with a compressive strength of 37.4 ± 5.2 MPa (height 20 mm) and 28.4 ± 10.1 MPa (height 6 mm), as shown in Figure 2A below. Accordingly, there was no significant difference between the two tested heights of the microporous β-TCP implant. As expected, both macroporous β-TCP implants showed a very low compressive strength of 1.4 ± 0.2 MPa (height 20 mm) and 1.1 ± 0.3 MPa (height 6 mm), which was significantly different from all other implants tested.

 doi:10.20944/preprints202405.0547.v1

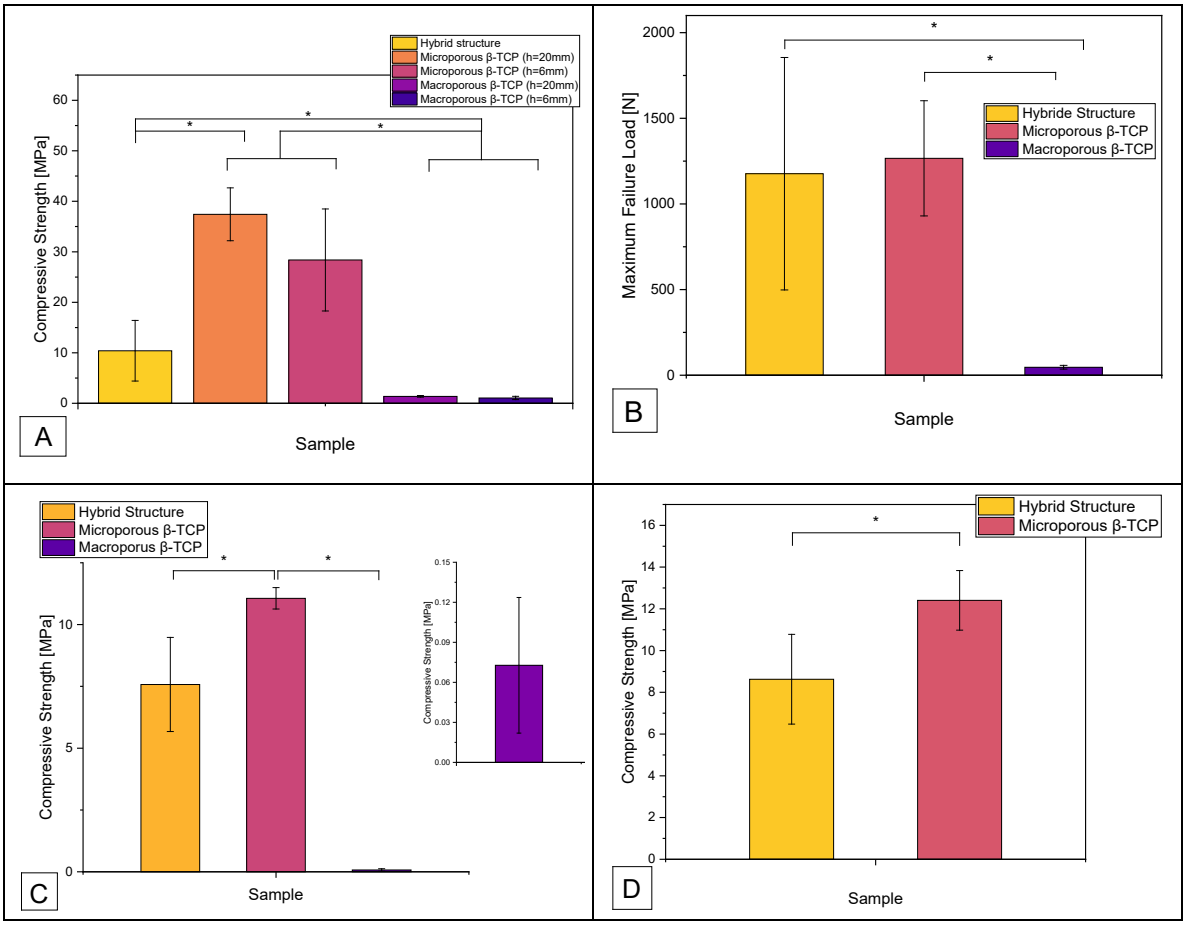

Figure 2. Overview of compressive strength and maximum failure load of the different samples; A: Compressive strength as a function of sample origin; B: Maximum failure loads of the samples; C: Compressive strength of samples of different origin (manufacturing process) after degradation test according to ISO EN 10993-14 in Tris buffer with pH 7.4 for 60 days; D: Compressive strength of β-TCP samples (different production) after degradation in Tris buffer with pH 5.0 for 60 days; (*) statistically significant difference with $p<0.05$.

The maximum failure load refers to the force in N that the implant withstood before fracture, regardless of the surface area and height of the implant. As shown in Figure 2B, the measurement of the maximum failure load showed a significant difference between the measured values of the hybrid structure of 1176.6 ± 678.7 N and the values of the macroporous β-TCP implant of 46.6 ± 11.1 N. The maximum failure load of the microporous β-TCP implant of 1266.4 ± 336.1 N was also significantly different from the measurement results of the macroporous implant. After degradation of the β-TCP implants in Tris buffer at pH 7.4 for 60 days, a significant difference ($p<0.05$) was observed between the compressive strength of the hybrid structure at 7.6 ± 1.9 MPa and that of the microporous β-TCP implant at 11.1 ± 0.4 MPa (see Figure 2C). The compressive strength of the macroporous β-TCP implant was 0.07 ± 0.05 MPa. Compared to the initial values of the respective β-TCP samples, the compressive strength of the microporous β-TCP scaffold decreased significantly by 66% after the degradation test in Tris buffer. In contrast, the compressive strength of the hybrid structure and the macroporous β-TCP scaffold showed no significant change (see Table 1). Figure 1D shows the compressive strength of the scaffolds after degradation in Tris buffer at pH 5 for 60 days. The microporous β-TCP implant showed a significantly higher compressive strength of 12.4 ± 1.4 MPa compared to the compressive strength of the hybrid structure of 8.6 ± 2.1 MPa. All results are summarized in Table 1 below.

 doi:10.20944/preprints202405.0547.v1

Table 1. Summary of the compressive strengths and maximum failure loads of the various β-TCP scaffolds produced (with/without incubation in TRIS).

Compressive Strength [MPa]			
Sample	Hybrid Structure	Microporous β-TCP	Macroporous β-TCP
No Tris buffer	10.4 ± 6	32.9 ± 8.7	1.2 ± 0.3
Tris buffer pH 7.4	7.6 ± 1.9	11.1 ± 0.4	0.07 ± 0.05
Tris buffer pH 5	8.6 ± 2.1	12.4 ± 1.4	n.a.
Maximum Failure Load [N]			
Sample	Hybrid Structure	Microporous β-TCP	Macroporous β-TCP
No Tris buffer	1176.6 ± 678.7	1266.4 ± 336.1	46.6 ± 11.1
Tris buffer pH 7.4	856.9 ± 215.4	425.7 ± 16.7	2.8 ± 2
Tris buffer pH 5	975.7 ± 243.1	477.5 ± 55	n.a.

3.3. Bicompatibility

3.3.1. Live/Dead-Assay

The following Figure 2 shows examples of fluorescence microscopic images of the surface of all samples, magnified 5 times in the overlay filter. Accordingly, the living cells fluoresce green and the red cells red. It is noticeable that the number of living cells increased over the 10-day experimental period. The number of cells per square millimeter on the surface of all samples increased continuously over the 10-day test period. From day 3 to day 7, the average cell count of all samples approximately doubled. As expected, the number of cells on the 2D control increased the most. The number of cells on the macroporous β-TCP scaffold showed the second largest increase, but with significantly lower values. The microporous β-TCP scaffold displayed a steeper increase in cell number than the hybrid structure. The increase in cell number of the 3D control was intermediate. Only in the case of the 2D control, the number of dead cells per square millimeter on the surface of the specimens increased progressively over the 10-day test period. In general, the number of dead cells was irrelevant in all samples (see Figure 3 and Table 2).

Table 2. Cells per mm² on the different scaffolds.

Surface	**day 3**		**day 7**		**day 10**	
Cells/mm²	**living**	**dead**	**living**	**dead**	**living**	**dead**
Hybrid structure	66 ± 22	2 ± 4	131 ± 66	3 ± 5	240 ± 84	1 ± 1
Microporous β-TCP	128 ± 136	1 ± 1	266 ± 270	1 ± 1	624 ± 462	1 ± 3
Macropoous β-TCP	256 ± 299	1 ± 1	520 ± 520	0	993 ± 748	3 ± 9
3D-control curasan	64 ± 70	9 ± 11	166 ± 101	12 ± 22	380 ± 216	6 ± 4
2D-control Thermanox	862 ± 548	3 ± 4	1697 ± 403	12 ± 15	2468 ± 420	50 ± 51

 doi:10.20944/preprints202405.0547.v1

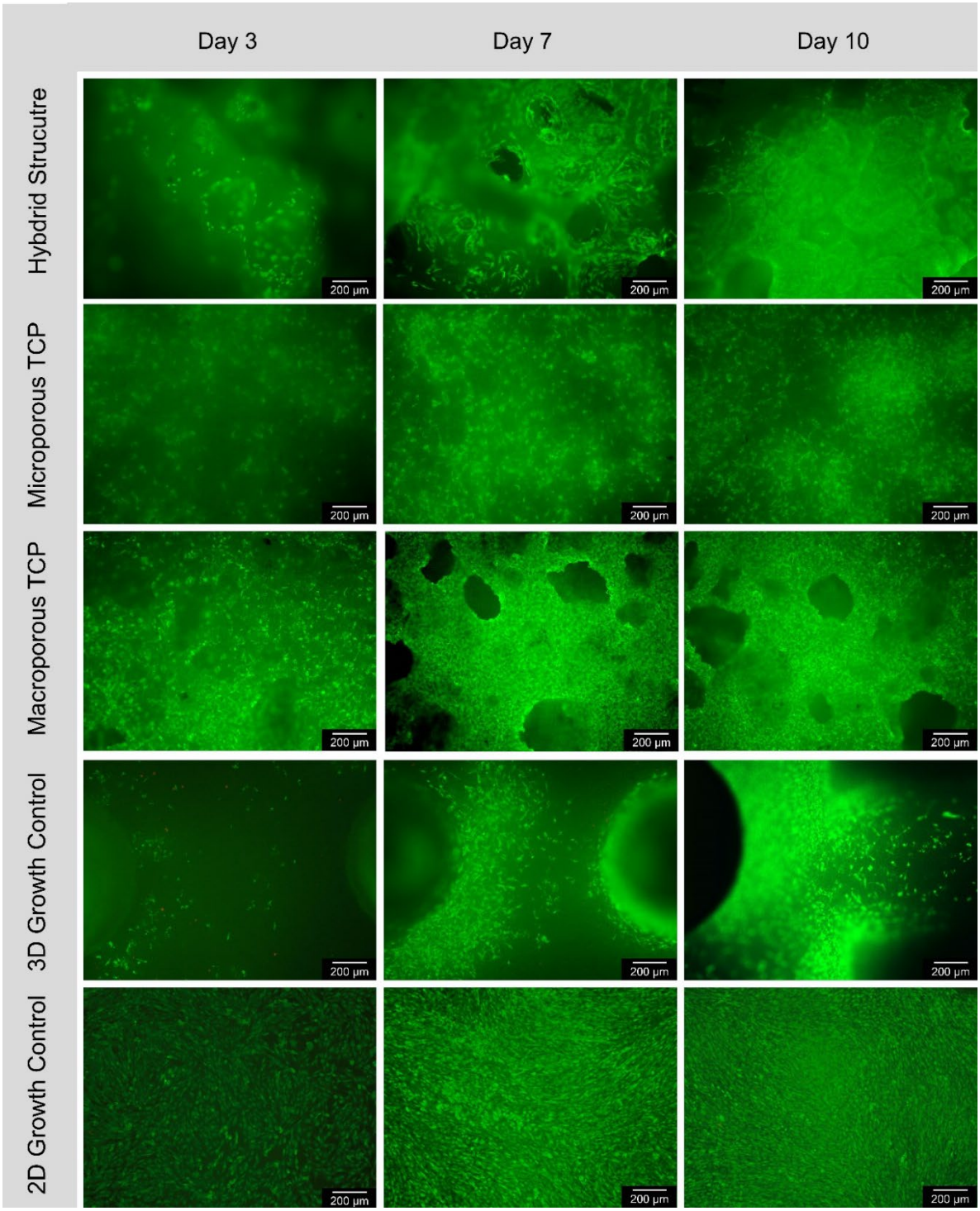

Figure 3. Course of cell growth on the surface according to 3, 7 and 10 days for Hybrid Structure; Microporous TCP; Macroporous TCP; 3D growth control and 2D growth control (Thermanox Coverslip); Images in 5x magnification, Images taken with Olympus BX-53 Fluorescence microscope.

3.3.2. Cell Proliferation (WST-I)

The extinction values measured in the cell proliferation assay with a wavelength of 450 nm showed an increase between the first measurement time after 3 days and after 10 days for all β-TCP implants and 2D control (see Figure 4A). The graph of the microporous β-TCP implant showed the slightest slope; between the extinction values measured after 3 and 7 days a definite increase cannot yet be determined. The same applies to the 3D control. As expected, the graph of the 2D control showed the largest increase.

 doi:10.20944/preprints202405.0547.v1

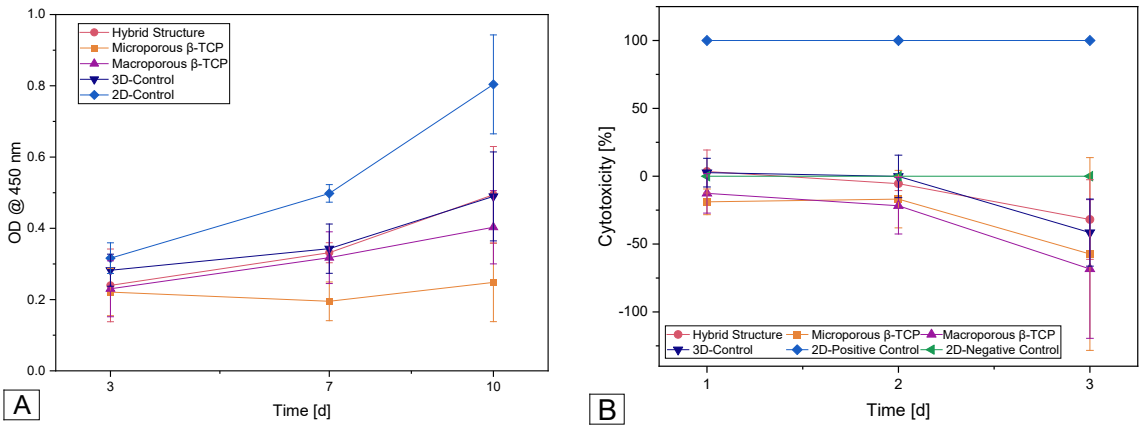

Figure 4. A: Cell proliferation after 3, 7 and 10 days on the different samples; B: Cytotoxicity curves of all samples after 1, 2 and 3 days.

3.3.3. Cytotoxicity (LDH)

The cytotoxicity of the scaffolds was 0% in almost all samples. Only the 3D cell controls and the hybrid structure started with 2.6% and 3.5% cytotoxicity, respectively, on day 1 and then became zero at the next test time point. The negative values on the curve in Figure 4B correspond to 0% cytotoxicity.

4. Discussion

4.1. Porosity

Based on the present results, the influence of porosity on the mechanical strength of β-TCP implants could be demonstrated. These findings are supported by those of other authors who also observed an inverse correlation between porosity and compressive strength of β-TCP implants [29–32]. Peralta et al. [33] specifically addressed this correlation in human bone: a 5% increase in porosity corresponded to a 20 MPa decrease in compressive strength, which is approximately 10% of the maximum compressive strength of human cortical bone samples. As mentioned above, the hybrid structure has a comparatively high compressive strength for its high porosity of 74.4%; accordingly, with the specific design of the column structure with macroporous filling based on the structure of human bone, the production of a predominantly microporous TCP scaffold with great mechanical resilience was successful.

4.2. Mechanical Properties

The measurement of the maximum failure load of the macroporous β-TCP implant stands in agreement with the previous investigations by Seidenstuecker et al. [28] and confirms the premise that the macroporous implant would only permit extremely limited use in load-bearing applications. Compared to the compressive strength of human cancellous bone of 15.9 ± 7.4 MPa [34], the measured compressive strength of the macroporous scaffold of 1.2 ± 0.3 MPa is well outside the calculated standard deviation of the compressive strength of human bone.

In the first study to validate the tested microporous β-TCP implant, its compressive strength was investigated by Mayr et al. [35]. The maximum failure load of the implant was determined using a Zwick 1486 servo-hydraulic universal compression testing machine (ZwickRoell GmbH & Co. KG, Ulm, Germany) with a 20kN load cell. The calculated compressive strength reflects the physiological conditions of the implant in the bone and was 79.19 ± 22.57 MPa.

In the case of the hybrid structure, the compressive strength measurement at 10.4 ± 6 MPa in the present paper differs from the results of Ahlhelm et al. [27] at 23 ± 4 MPa. This could be explained by the use of different measuring devices, the number of samples and the environmental conditions. Ahlhelm et al. [27] performed their measurements using the Instron 8562 universal testing machine

 doi:10.20944/preprints202405.0547.v1

(Illinois Tool Works Inc., Norwood, USA). The results suggest that the hybrid structure's compressive strength is similar to that of human cancellous bone. Furthermore, the increased values for the compressive strength of the microporous β-TCP implant at 32.9 ± 8.7 MPa are similar to the values of Seidenstuecker et al. [28] at 24 ± 6 MPa. Accordingly, the compressive strength of the microporous β-TCP implant exceeds the compressive strength of human cancellous bone, which is assumed to be at 15.9 ± 7.4 MPa [34]. In terms of compressive strength, the measured values of the hybrid structure match the reference values of human cancellous bone and allow the assumption that this β-TCP implant can be used as an adequate replacement for cancellous bone in terms of mechanical strength. This is also suggested by the measured values of the microporous β-TCP implant, which are higher than those of human cancellous bone. However, human bone is known to consist of cancellous bone surrounded by cortical bone, which differs in its mechanical properties from cancellous bone. The suitability of a bone implant must therefore be tested or selected specifically for its intended use. For example, the requirements for the implant are different if it is to be implanted within the intact cortical scaffold of a long bone, as a complete replacement of a long bone, or in a flat bone such as the pelvis.

The literature describes a decrease in the compressive strength of cortical bone depending on temperature and pressure applied orthogonally to the direction of the Haversian canals. At a temperature of 38.5°C, the compressive strength of compact bone decreases from 82.7 ± 11.3 MPa, measured in the direction of the Haversian canals, to 67.6 ± 10.9 MPa orthogonally [36]. Data on the compressive strength of human compact bone varies between values of 130 and 180 MPa [33,37]. As a result, the measured compressive strength values of all β-TCP implants tested in the present study were found to be well below the reference value for the compressive strength of human cortical bone. Therefore, it can be assumed that the tested β-TCP implants would not be suitable for an immediately load-bearing application as an implant in the case of a critical bone substance defect with a loss of compact bone. However, given the compressive strength of the hybrid structure, which is comparable to that of human cancellous bone, there is reason to believe that they could be used in cases of planned autologous cancellous bone grafting or as an addition to insufficient autograft material. Mayr et al. [35] found in a large animal study that the microporous β-TCP implants with preoperatively applied autologous chondrocytes were resorbed on average by 74% after 6 months and on average by 81% after 12 months.

The initially empty defect showed 15% bone content after 6 months, while 32% of the defect filled with the β-TCP implant had been converted to bone, as reported by Bernstein et al. [38] in the same study. The β-TCP implants were replaced by cancellous bone instantaneously, which was formed depending on its load according to Wolff's law. Based on these findings, a more concrete statement can be made regarding the load-bearing applicability of the microporous β-TCP implant. The resorption and bone ingrowth behavior of the microporous β-TCP implant appears to be beneficial to the healing of osteochondral defects and to provide a better result in terms of resulting bone quality and quantity than a non-treated empty defect. With regard to the hybrid structure, no concrete statements can be made regarding the load-bearing applicability of the implant, as the hybrid structure was inserted subdermally in the present in vivo study [27]. However, it can be assumed that the hybrid structure, due to its mechanical strength comparable to that of human cancellous bone and its manufacturing from pure beta-TCP, would exhibit similar resorption and bone ingrowth behavior as the microporous beta-TCP implant and could therefore be used in a load-bearing capacity. In synopsis with the literature, the values obtained for the compressive strength of the hybrid structure, considering the high porosity of the β-TCP implant, are at the top of the range of the comparative values. With its porosity of 74.4% the hybrid structure shows a higher compressive strength compared to the 3D-printed β-TCP implants of Santos et al. [39] with a porosity of 54.4%, produced at the same sintering temperature as the hybrid structure: 10.4 ± 6 MPa compared to 2.36 ± 0.05 MPa. When the sintering temperature was increased to 1400°C with a porosity of 46.1%, Santos et al. [39] obtained comparable compressive strength values of 8.66 ± 0.11 MPa. Respecting a slow cooling process, the increased sintering temperature only increased the crystallinity of β-TCP but did not induce a phase transformation to α-TCP; the authors support their statements with an X-ray

 doi:10.20944/preprints202405.0547.v1

diffraction analysis. Tarafder et al. [40] also reported corresponding values for their 3D printed microwave sintered β-TCP implants with a compressive strength of 10.95 ± 1.28 MPa and a porosity of 42%. Liu et al. [32] produced 3D printed β-TCP implants with a relatively low compressive strength of 0.8 MPa up to a maximum of 4.1 MPa, which they achieved by adjusting the porosity from 75% to 45% and the pore size from 1200 µm to 360 µm. The currently highest compressive strength values for 3D printed β-TCP implants were reported by Schmidleithner et al. [31]: The linear lattice structure showed a compressive strength of 44.7 MPa at a porosity of 50%. When the porosity was increased to 75%, the reported value was reduced to 14.2 MPa. The compressive strength of the hexagonal Kagome structure was 19.5 MPa and 6.75 MPa, at 50% and 75% porosity respectively. Schmidleithner et al. [31] also refer to the phenomenon of microcracks in β-TCP. Among other things, these microcracks could be responsible for the large mean variation of these measured values, since they can lead to premature material fractures during printing [41]. Bertrand et al. [42] also reported this problem regarding the humidification of their 3D printed β-TCP implants during the printing process. Using a 3D bioplotter, they produced cylindrical, multilayer β-TCP implants with a layer rotation of 1°, which withheld between 14.97 ± 1.08 MPa and 41.6 ± 7.12 MPa at a porosity of 38.8%. The maximum values were achieved with a 12-layer β-TCP implant printed with a 0.25 mm needle diameter after pretreatment in PBS. The compressive strength of the microporous β-TCP implant was significantly higher than the hybrid structure´s. This was to be expected given the higher porosity of the hybrid structure, although the implant is at the upper end of the literature range in terms of compressive strength. Clearly, there are significant differences between the different manufacturing processes of β-TCP implants with respect to the mechanical strength of the implants. In the degradation test, there was no significant change between the compressive strength before and after the degradation test in Tris buffer at pH 7.4 for 60 days in the hybrid structure and the macroporous β-TCP implant. On the other hand, the compressive strength of the microporous β-TCP implant showed a significant reduction of 66% after the degradation test in Tris buffer at pH 7.4 for 60 days. Even after the degradation test in Tris buffer at pH 5, the measured value for the compressive strength of the hybrid structure does not differ significantly from the comparative value before the degradation test, while the compressive strength of the microporous β-TCP implant after degradation in Tris buffer at pH 5 for 60 days showed a significant decrease of 62% to 12.4 ± 1.4 MPa compared to the initial value before the degradation test. With regard to the macroporous β-TCP implant, it can be assumed that it would withstand a compressive load only under physiological conditions; there was no significant change in compressive strength after degradation in Tris buffer at pH 7.4 for 60 days compared to the initial value. After degradation in Tris buffer at pH 5 for 60 days however, the macroporous β-TCP implant was degraded, so it can be assumed that the implant would not remain dimensionally stable in inflamed tissue. The absence of a significant reduction in the compressive strength of the hybrid structure after degradation in Tris buffer at pH 7.4 and pH 5 for 60 days supports the usability of this implant both in the physiological pH range of human blood as well as in the acid pH range of inflamed tissue. The significant reduction in compressive strength of the microporous β-TCP implant after the degradation test in Tris buffer with pH 7.4 for 60 days as well as in Tris buffer with pH 5 illustrates that the material properties of the implant change under physiological and inflammatory conditions, in particular the compressive strength decreases. Since the initial compressive strength value of the microporous beta-TCP implant is greater than the comparative compressive strength value of human bone and even after the degradation test its compressive strength is similar to the reference value of human bone, the microporous beta-TCP implant can nevertheless be considered for load-bearing applications under physiological and inflammatory conditions. It should be noted that the degradation test was performed with an incubation period of 60 days, whereas the cell culture only allowed for a study up to a maximum duration of 10 days. This limitation of the cell culture leads to a noticeable deficit in data acquisition in the period of peri- and intra-implant bone regeneration, which for β-TCP extends over a total of more than 6 months [43]. In direct comparison, it was shown that the compressive strength of the hybrid structure did not decrease under physiological and inflammatory conditions, whereas that of the microporous β-TCP implant experienced a significant reduction. The surprising finding of the

 doi:10.20944/preprints202405.0547.v1

lower pH sensitivity of the hybrid structure suggests that the foam of the hybrid structure, with its lower interconnectivity than the pores of the microporous β-TCP implant, exhibits a better sealed surface, which allows for less acid to penetrate.

4.3. Biocompatibility

Cell proliferation was detected on all β-TCP implants within 10 days using the cell proliferation assay and the live/dead assay. This observation is consistent with the results of Ahlhelm et al. [27] and Mayr et al. [24] , who characterized the hybrid structure and the microporous β-TCP implant as cell proliferation promoting and osteoconductive, respectively. In comparison, the microporous β-TCP implant showed a greater increase in cell number than the hybrid structure. One explanation for this may be that the cells migrated into the interior of the 3D construct due to the high porosity of the hybrid structure, meaning that a direct comparison of the increase in cell count over time in relation to the surface of the construct may not be meaningful. It was found that cells did not migrate into the microporous β-TCP implant, but only into the macroporous β-TCP implant and the hybrid structure. This was an expected result because the cells used do not fit into the micropores due to their size. There was also an increase in the number of cells located within the 3D constructs. Only a few cells could be seen on the edge of the hybrid structure, i.e., on the microporous columnar structure.

This is consistent with the findings of Ghanaati et al. [44], who found that macropores combined with high overall implant porosity favored ingrowth of cells and connective tissue fibers into the center of the β-TCP implant. Consequently, cell proliferation occurs on both the microporous β-TCP implant and the hybrid structure. However, the key difference is that numerous cells grow into the hybrid structure and proliferate within the construct. The hybrid structure proved to be extremely hygroscopic, i.e., during cell seeding it was observed that the cell fluid was virtually sucked into the interior of the implant and no droplets formed on the surface of the implant, as was the case with the other implants, except for the 3D control. This is a known phenomenon that Seidenstücker et al. [45] have already described with their β-TCP implants. This phenomenon is caused by the high total porosity of the hybrid structure of 74.4 ± 0.5% and the macropores of 0.1-0.6 mm diameter in the freezing foam.

As expected, the results of the lactate dehydrogenase assay with maximum cytotoxicity values of less than 20% at all time points for all β-TCP implants indicate that the tested β-TCP implants are not cytotoxic. This is consistent with the data collected by Ahlhelm et al. [27] and Bernstein et al. [24]. In the context of the existing studies on the biocompatibility of β-TCP [27,46] and the present results, it can be assumed that the investigated β-TCP implants are not cytotoxic and allow cell proliferation on their surface. Therefore, the implants can be defined as osteoconductive.

From a methodological point of view, the partially negative percentages of cytotoxicity can be explained by the experimental design. In the case of the two-dimensional negative control, the drop of cell fluid was placed on the membrane and then incubated. On the 3D constructs, however, the drop of cell fluid could not be placed in such a way as to exclude the presence of cells at the bottom of the well. In order to be able to make a statement only about the cells on the 3D constructs, these were transferred to a new well after the drop of cell fluid had been placed. As a result, it is possible that there were initially fewer cells on the 3D constructs than on the negative control. The cells in the negative control may have proliferated to the point where there was insufficient space and medium for them to survive, resulting in more cells dying than on the 3D constructs. In the calculation of cytotoxicity, the value of the negative control is subtracted from the measured value of the sample; accordingly, the percentage value for cytotoxicity is negative if the measured value of the sample is lower than the value of the negative control. As mentioned above, the negative values were considered to be zero.

5. Conclusions

Both the conventionally fabricated microporous β-TCP scaffold and the 3D printed implant are suitable for bone replacement in load-bearing applications. In addition, both β-TCP scaffolds were found to be biocompatible and osteoconductive, as expected because of their manufacturing from β-

TCP. In order to thoroughly assess the potential of the two β-TCP scaffolds for bone replacement in load-bearing applications, further studies over a longer period of time are required to observe the resorption and bone ingrowth behavior of the implants, including histological examination, to ensure the mechanical load-bearing capacity of the implants during the bone remodeling process. The shear strength of the two implants could also be studied in more detail.

Author Contributions: Author Contributions: Conceptualization, H.O.M. and M.S.; methodology, M.S.; software, M.S., H.S.; validation, T.Z., M.A. and M.S.; formal analysis, T.Z., M.S.; investigation, T.Z., M.A. and M.S.; resources, H.S. and H.O.M..; data curation, T.Z. and M.S..; writing original draft preparation, M.S. and T.Z..; writing review and editing, M.S. and T.Z..; visualization, T.Z.; supervision, M.S.; project administration, M.S:; funding acquisition, M.S. All authors have read and agreed to the published version of the manuscript

Funding: The article processing charge was funded by the Baden-Wuerttemberg Ministry of Science, Research and Art and the University of Freiburg in the funding program Open Access Publishing.

Institutional Review Board Statement: Not applicable

Informed Consent Statement: Not applicable

Data Availability Statement: The data presented in this study are available on request from the corresponding author.

Acknowledgments: We would like to dedicate this work to Prof. Bernstein, who was the initiator of this work, but who unfortunately passed away much too early in an accident in the summer of 2021.

Conflicts of Interest: The authors declare no conflicts of interest.

References

1. Nauth, A.; Schemitsch, E.; Norris, B.; Nollin, Z.; Watson, J.T. Critical-size bone defects: Is there a consensus for diagnosis and treatment? *J Orthop Trauma* **2018**, *32 Suppl 1*, S7-s11.https://doi.org/10.1097/bot.0000000000001115
2. Keating, J.F.; Simpson, A.H.; Robinson, C.M. The management of fractures with bone loss. *J Bone Joint Surg Br* **2005**, *87*, 142-150.https://doi.org/10.1302/0301-620x.87b2.15874
3. Kaatsch, P. Epidemiology of childhood cancer. *Cancer Treat Rev* **2010**, *36*, 277-285.https://doi.org/10.1016/j.ctrv.2010.02.003
4. Fornetti, J.; Welm, A.L.; Stewart, S.A. Understanding the bone in cancer metastasis. *J. Bone Miner. Res.* **2018**, *33*, 2099-2113.https://doi.org/10.1002/jbmr.3618
5. Omar, M.; Graulich, T.; von Falck, C.; Bruns, N.; Krettek, C.; Ettinger, M. Versorgungsstrategien bei tumorbedingten pathologischen frakturen der extremitäten. *Der Unfallchirurg* **2021**, *124*, 704-719.https://doi.org/10.1007/s00113-021-01056-w
6. Azi, M.L.; Aprato, A.; Santi, I.; Kfuri, M., Jr.; Masse, A.; Joeris, A. Autologous bone graft in the treatment of post-traumatic bone defects: A systematic review and meta-analysis. *BMC Musculoskelet Disord* **2016**, *17*, 465.https://doi.org/10.1186/s12891-016-1312-4
7. destatis. Fallpauschalenbezogene krankenhausstatistik (drg-statistik) operationen und prozeduren der vollstationären patientinnen und patienten in krankenhäusern (4-steller) für 2021. Office, G.F.S., Ed. Wiesbaden, 2022;
8. Kim, D.H.; Rhim, R.; Li, L.; Martha, J.; Swaim, B.H.; Banco, R.J.; Jenis, L.G.; Tromanhauser, S.G. Prospective study of iliac crest bone graft harvest site pain and morbidity. *Spine J* **2009**, *9*, 886-892.https://doi.org/10.1016/j.spinee.2009.05.006
9. Dimitriou, R.; Mataliotakis, G.I.; Angoules, A.G.; Kanakaris, N.K.; Giannoudis, P.V. Complications following autologous bone graft harvesting from the iliac crest and using the ria: A systematic review. *Injury* **2011**, *42*, S3-S15.https://doi.org/10.1016/j.injury.2011.06.015
10. Harris, M.; Chung, F. Complications of general anesthesia. *Clin Plast Surg* **2013**, *40*, 503-513.https://doi.org/10.1016/j.cps.2013.07.001
11. Lohmann, H.; Grass, G.; Rangger, C.; Mathiak, G. Economic impact of cancellous bone grafting in trauma surgery. *Arch Orthop Trauma Surg* **2007**, *127*, 345-348.https://doi.org/10.1007/s00402-006-0277-4
12. Rupp, M.; Klute, L.; Baertl, S.; Walter, N.; Mannala, G.K.; Frank, L.; Pfeifer, C.; Alt, V.; Kerschbaum, M. The clinical use of bone graft substitutes in orthopedic surgery in germany-a 10-years survey from 2008 to 2018 of 1,090,167 surgical interventions. *J. Biomed. Mater. Res. B Appl. Biomater.* **2022**, *110*, 350-357.https://doi.org/10.1002/jbm.b.34911

13. Girón, J.; Kerstner, E.; Medeiros, T.; Oliveira, L.; Machado, G.M.; Malfatti, C.F.; Pranke, P. Biomaterials for bone regeneration: An orthopedic and dentistry overview. *Braz. J. Med. Biol. Res.* **2021**, *54*, e11055.https://doi.org/10.1590/1414-431X2021e11055
14. Khijmatgar, S.; Panda, S.; Das, M.; Arbildo-Vega, H.; Del Fabbro, M. Recombinant factors for periodontal intrabony defects: A systematic review and network meta-analysis of preclinical studies. *J Tissue Eng Regen Med* **2021**, *15*, 1069-1081.https://doi.org/10.1002/term.3250
15. Battafarano, G.; Rossi, M.; De Martino, V.; Marampon, F.; Borro, L.; Secinaro, A.; Del Fattore, A. Strategies for bone regeneration: From graft to tissue engineering. *Int J Mol Sci* **2021**, *22*.https://doi.org/10.3390/ijms22031128
16. Filardo, G.; Kon, E.; Tampieri, A.; Cabezas-Rodríguez, R.; Di Martino, A.; Fini, M.; Giavaresi, G.; Lelli, M.; Martínez-Fernández, J.; Martini, L., et al. New bio-ceramization processes applied to vegetable hierarchical structures for bone regeneration: An experimental model in sheep. *Tissue Eng Part A* **2014**, *20*, 763-773.https://doi.org/10.1089/ten.TEA.2013.0108
17. Manfrini, M.; Di Bona, C.; Canella, A.; Lucarelli, E.; Pellati, A.; D'Agostino, A.; Barbanti-Bròdano, G.; Tognon, M. Mesenchymal stem cells from patients to assay bone graft substitutes. *J Cell Physiol* **2013**, *228*, 1229-1237.https://doi.org/10.1002/jcp.24276
18. Dong, X.; Xu, X. Bioceramics in endodontics: Updates and future perspectives. *Bioengineering (Basel, Switzerland)* **2023**, *10*.https://doi.org/10.3390/bioengineering10030354
19. Bohner, M.; Santoni, B.L.G.; Döbelin, N. B-tricalcium phosphate for bone substitution: Synthesis and properties. *Acta Biomater.* **2020**, *113*, 23-41.https://doi.org/10.1016/j.actbio.2020.06.022
20. Galois, L.; Mainard, D.; Delagoutte, J.P. Beta-tricalcium phosphate ceramic as a bone substitute in orthopaedic surgery. *Int Orthop* **2002**, *26*, 109-115.https://doi.org/10.1007/s00264-001-0329-x
21. Köster, K.; Karbe, E.; Kramer, H.; Heide, H.; König, R. [experimental bone replacement with resorbable calcium phosphate ceramic (author's transl)]. *Langenbecks Arch Chir* **1976**, *341*, 77-86.https://doi.org/10.1007/bf01262779
22. Hirata, M.; Murata, H.; Takeshita, H.; Sakabe, T.; Tsuji, Y.; Kubo, T. Use of purified beta-tricalcium phosphate for filling defects after curettage of benign bone tumours. *Int Orthop* **2006**, *30*, 510-513.https://doi.org/10.1007/s00264-006-0156-1
23. Seto, S.; Muramatsu, K.; Hashimoto, T.; Tominaga, Y.; Taguchi, T. A new β-tricalcium phosphate with uniform triple superporous structure as a filling material after curettage of bone tumor. *Anticancer Res.* **2013**, *33*, 5075-5081
24. Bernstein, A.; Nobel, D.; Mayr, H.O.; Berger, G.; Gildenhaar, R.; Brandt, J. Histological and histomorphometric investigations on bone integration of rapidly resorbable calcium phosphate ceramics. *J. Biomed. Mater. Res. B Appl. Biomater.* **2008**, *84*, 452-462.https://doi.org/10.1002/jbm.b.30891
25. Mayr, H.O.; Suedkamp, N.P.; Hammer, T.; Hein, W.; Hube, R.; Roth, P.V.; Bernstein, A. B-tricalcium phosphate for bone replacement: Stability and integration in sheep. *J. Biomech.* **2015**, *48*, 1023-1031.https://doi.org/10.1016/j.jbiomech.2015.01.040
26. Seidenstuecker, M.; Mrestani, Y.; Neubert, R.H.H.; Bernstein, A.; Mayr, H.O. Release kinetics and antibacterial efficacy of microporous β-tcp coatings. *Journal of Nanomaterials* **2013**, *2013*, 8.https://dx.doi.org/10.1155/2013/842951
27. Ahlhelm, M.; Latorre, S.H.; Mayr, H.O.; Storch, C.; Freytag, C.; Werner, D.; Schwarzer-Fischer, E.; Seidenstücker, M. Mechanically stable β-tcp structural hybrid scaffolds for potential bone replacement. *Journal of Composites Science* **2021**, *5*, 281.https://doi.org/10.3390/jcs5100281
28. Seidenstuecker, M.; Schmeichel, T.; Ritschl, L.; Vinke, J.; Schilling, P.; Schmal, H.; Bernstein, A. Mechanical properties of the composite material consisting of β-tcp and alginate-di-aldehyde-gelatin hydrogel and its degradation behavior. *Materials* **2021**, *14*, 1303.https://doi.org/10.3390/ma14051303
29. Yamasaki, H.; Sakai, H. Osteogenic response to porous hydroxyapatite ceramics under the skin of dogs. *Biomaterials* **1992**, *13*, 308-312
30. Yuan, H.; Fernandes, H.; Habibovic, P.; de Boer, J.; Barradas, A.M.; de Ruiter, A.; Walsh, W.R.; van Blitterswijk, C.A.; de Bruijn, J.D. Osteoinductive ceramics as a synthetic alternative to autologous bone grafting. *Proc Natl Acad Sci U S A* **2010**, *107*, 13614-13619.https://doi.org/10.1073/pnas.1003600107
31. Schmidleithner, C.; Malferrari, S.; Palgrave, R.; Bomze, D.; Schwentenwein, M.; Kalaskar, D.M. Application of high resolution dlp stereolithography for fabrication of tricalcium phosphate scaffolds for bone regeneration. *Biomed Mater* **2019**, *14*, 045018.https://doi.org/10.1088/1748-605X/ab279d
32. Liu, S.; Chen, J.; Chen, T.; Zeng, Y. Fabrication of trabecular-like beta-tricalcium phosphate biomimetic scaffolds for bone tissue engineering. *Ceramics International* **2021**, *47*, 13187-13198.https://doi.org/10.1016/j.ceramint.2021.01.184
33. Peralta, L.; Maeztu Redin, J.D.; Fan, F.; Cai, X.; Laugier, P.; Schneider, J.; Raum, K.; Grimal, Q. Bulk wave velocities in cortical bone reflect porosity and compression strength. *Ultrasound Med Biol* **2021**, *47*, 799-808.https://doi.org/10.1016/j.ultrasmedbio.2020.11.012

34. Perilli, E.; Baleani, M.; Öhman, C.; Fognani, R.; Baruffaldi, F.; Viceconti, M. Dependence of mechanical compressive strength on local variations in microarchitecture in cancellous bone of proximal human femur. *J Biomech* **2008**, *41*, 438-446.https://doi.org/10.1016/j.jbiomech.2007.08.003
35. Mayr, H.O.; Suedkamp, N.P.; Hammer, T.; Hein, W.; Hube, R.; Roth, P.V.; Bernstein, A. Beta-tricalcium phosphate for bone replacement: Stability and integration in sheep. *J. Biomech.* **2015**, *48*, 1023-1031.https://doi.org/10.1016/j.jbiomech.2015.01.040
36. Ma, Z.; Qiang, Z.; Zhao, H.; Piao, H.; Ren, L. Mechanical properties of cortical bones related to temperature and orientation of haversian canals. *Materials Research Express* **2020**, *7*, 015408.https://doi.org/10.1088/2053-1591/ab6899
37. Wagoner Johnson, A.J.; Herschler, B.A. A review of the mechanical behavior of cap and cap/polymer composites for applications in bone replacement and repair. *Acta Biomater* **2011**, *7*, 16-30.https://doi.org/10.1016/j.actbio.2010.07.012
38. Bernstein, A.; Niemeyer, P.; Salzmann, G.; Südkamp, N.P.; Hube, R.; Klehm, J.; Menzel, M.; von Eisenhart-Rothe, R.; Bohner, M.; Görz, L., et al. Microporous calcium phosphate ceramics as tissue engineering scaffolds for the repair of osteochondral defects: Histological results. *Acta Biomater* **2013**, *9*, 7490-7505.https://doi.org/10.1016/j.actbio.2013.03.021
39. Santos, C.F.; Silva, A.P.; Lopes, L.; Pires, I.; Correia, I.J. Design and production of sintered β-tricalcium phosphate 3d scaffolds for bone tissue regeneration. *Mater Sci Eng C* **2012**, *32*, 1293-1298
40. Tarafder, S.; Balla, V.K.; Davies, N.M.; Bandyopadhyay, A.; Bose, S. Microwave-sintered 3d printed tricalcium phosphate scaffolds for bone tissue engineering. *J Tissue Eng Regen Med* **2013**, *7*, 631-641.https://doi.org/10.1002/term.555
41. Miranda, P.; Pajares, A.; Saiz, E.; Tomsia, A.P.; Guiberteau, F. Mechanical properties of calcium phosphate scaffolds fabricated by robocasting. *J Biomed Mater Res A* **2008**, *85A*, 218-227.https://doi.org/10.1002/jbm.a.31587
42. Bertrand, E.; Zankovic, S.; Vinke, J.; Schmal, H.; Seidenstuecker, M. About the mechanical strength of calcium phosphate cement scaffolds. *Designs* **2023**, *7*, 87.https://doi.org/10.3390/designs7040087
43. Zerbo, I.R.; Zijderveld, S.A.; de Boer, A.; Bronckers, A.L.; de Lange, G.; ten Bruggenkate, C.M.; Burger, E.H. Histomorphometry of human sinus floor augmentation using a porous beta-tricalcium phosphate: A prospective study. *Clin Oral Implants Res* **2004**, *15*, 724-732.https://doi.org/10.1111/j.1600-0501.2004.01055.x
44. Ghanaati, S.; Barbeck, M.; Orth, C.; Willershausen, I.; Thimm, B.W.; Hoffmann, C.; Rasic, A.; Sader, R.A.; Unger, R.E.; Peters, F., et al. Influence of β-tricalcium phosphate granule size and morphology on tissue reaction in vivo. *Acta Biomater* **2010**, *6*, 4476-4487.https://doi.org/10.1016/j.actbio.2010.07.006
45. Seidenstuecker, M.; Lange, S.; Esslinger, S.; Latorre, S.H.; Krastev, R.; Gadow, R.; Mayr, H.O.; Bernstein, A. Inversely 3d-printed β-tcp scaffolds for bone replacement. *Materials* **2019**, *12*, 3417.https://doi.org/10.3390/ma12203417
46. Seidenstuecker, M. Herstellung eines kompositmaterials bestehend aus einer porösen β -tricalciumphosphatkeramik und einem drug-release-system mit kontinuierlicher wirkstofffreisetzung. Dissertation, Universität Freiburg, 2015.https://doi.org/10.6094/UNIFR/10383